Grain-scale study of pile installation and subsequent axial loading cycles

J. Doreau-Malioche, G. Combe, J.B. Toni & G. Viggiani
Univ. Grenoble Alpes, CNRS, Grenoble INP (Institute of Engineering Univ. Grenoble Alpes), 3SR, Grenoble, France

ABSTRACT: The mechanisms occurring at the grain scale at sand-pile interface during pile installation and axial cyclic loading are analysed quantitatively in a mini calibration chamber, using X-ray tomography and advanced image analysis tools. Grain kinematics, porosity and grains orientations are studied, along with the macroscopic mechanical response of the interface. The test conditions are not representative of real engineering applications, where piles supporting bridges, tidal or wind turbines have to safely sustain severe load-controlled cycles. However, measurements at the grain scale shed light on the mechanisms controlling the macroscopic behaviour of sand-pile interface such as local density changes, grain kinematics and grains orientations.

1 INTRODUCTION

The mechanisms controlling the macroscopic behaviour of sand-pile interface during pile installation and axial cyclic loading are complex and are difficult to fully understand from field observations or from external measurements on laboratory-scale models.
Numerous experimental investigations have been reported on related topics of sand kinematics, grain crushing, local porosity changes, local effective stress changes and the macroscopic interface behaviour (White & Bolton 2002, Yang et al. 2010, Tsuha et al. 2012, Silva et al. 2013, Arshad et al. 2014). Even though the results greatly participated in the understanding of the mechanisms driving the interface global response, the observations were conducted either *post-mortem* or in plane strain and mainly during pile installation.
The present work focuses on the sand grains behaviour in the vicinity of the pile during pile installation and subsequent axial loading cycles. The tests were performed in a mini-calibration chamber installed in an x-ray scanner. The pile was installed by jacking and submitted to 1000 displacement-controlled cycles under constant radial stress. The tests do not represent accurately real engineering applications, where piles supporting bridges, tidal or wind turbines are subjected to load-controlled cycles due to their environment. However, the combined use of three-dimensional (3D) tomographic imaging and advanced tools such as 3D-digital image correlation (DIC), provides quantitative information at the grain scale and offers valuable data set against which theoretical or numerical approaches can be tested.

2 EXPERIMENTAL SETUP

The tests were carried out inside the x-ray scanner of Laboratoire 3SR. The mini-calibration chamber is a cylindrical cell transparent to x-rays in order to image phenomena while running a test (Fig. 1). The soil used for this study is Glageon sand, whose index properties are summarised in Table 1. Glageon sand is a calcareous sand derived from limestone rock crushed in Bocahut quarry, France, with $D_{50} = 1.125$ mm and a relatively uniform grading (between 1 mm and 1.25 mm). The angular and elongated shape of the grains of Glageon sand makes them highly crushable, which is the main reason they were selected for this study.
The samples tested, cylindrical with a diameter of 70 mm and a height of 128 mm, were prepared dry with an initial relative density ranging from 80% to 110%. At this relative density, triaxial compression tests gave φ' values of 48°.
An aluminium tubular model pile with an external diameter of 14 mm was used. The pile tip was conical (60°) and instrumented with strain gauges to record pile tip resistance. A load cell was mounted on the pile head to measure the total load (or head load) applied on the pile. Shaft resistance was estimated by subtracting the tip load from the total load. The model pile had a smooth surface with a roughness of about 0.7 μm. The roughness of sand-pile interface is known to be one of the most important factors affecting the unit shaft resistance (Fioravante 2002, Hebeler et al. 2015, Tehrani et al. 2016). Therefore, in the present study, the friction mobilised by the shaft is lower than the one measured in the field. Direct shear tests on sand-aluminium interface gave $\delta' = 15°$

whereas field piles have a roughness that leads to a typical δ' of about $30°$.

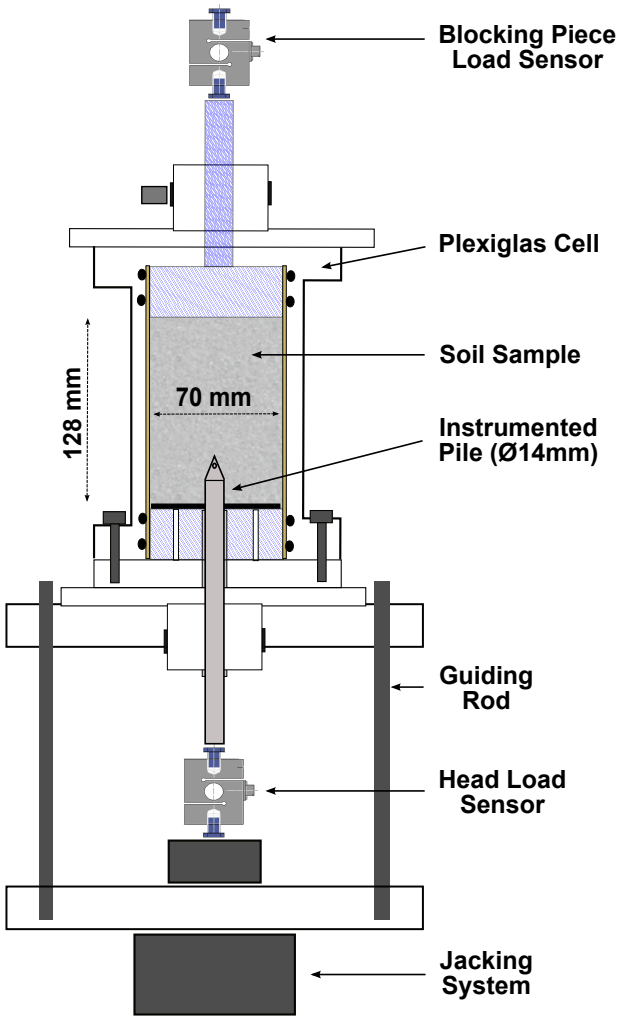

Figure 1. Schematic arrangement of the mini-calibration chamber.

3 X-RAY TOMOGRAPHY AND IMAGE ANALYSIS

3D images were acquired during pile installation and during cyclic loading after a certain number of cycles: 1, 50, 100, 500 and 1000. For the characterisation of the sample throughout a test, scans were recorded in 'global' tomography, *i.e.*, with a field of view containing the whole sample. However, the grain-scale analyses were done by acquiring images in 'local' tomography, i.e. with a field of view focused on the tip and the shaft, for a voxel size of 40 μm (which means that there are about 25 voxels across a grain diameter). A 3D rendering of the sand-pile interface recorded in 'local' tomography during pile embedment is shown in Figure 2.

The first analysis extracted from the x-ray images was the 3D field of porosity. The measurement of porosity was based on a binarisation of the grey-scale images, *i.e.*, a threshold was selected such that voxels with a grey level above this threshold were considered to be within the solid phase and those below this threshold within the void phase. Local porosity was calculated within a cubic window of 50 $voxel^3$ (containing about 30 grains) selected as the best compromise for a satisfactory representative elementary volume.

Fields of displacement were obtained thanks to 3D-DIC, which is essentially a powerful tool for assessing the spatial transformation between two digital images, here tomographies. In this work, a discrete version of the 3D-DIC code TomoWarp2 (Tudisco et al. 2017), recently developed at Laboratoire 3SR, was used. The main difference with the classical continuum approach is that the correlation window is replaced by subsets centered on individual grains that follow the actual shape of the grains and include only a single grain. Discrete DIC allows the measurement of the kinematics of each individual sand grain in the sample and takes into account possible discontinuities in displacement between the grains.

4 MACROSCOPIC RESPONSE OF THE INTERFACE

4.1 *Pile installation*

The pile was installed at a constant displacement rate of 25 μm/s until an initial embedment depth of 50 mm) under a confining pressure of 100 kPa. For practical reasons, the pile was installed from the bottom of cell, i.e. it moves upwards. A sketch of a typical head load profile during pile installation is given in Figure 2. The installation was studied by acquiring images after small increments of pile penetration of 1.0 mm (displacement of the pile tip).

4.2 *Cyclic loading*

Following the installation, the pile was submitted to a thousand axial displacement-controlled loading cycles. The cycles were performed at the same displacement rate as for the installation with an amplitude of $\pm$0.5 mm, alternating between compression and tension phases (two-way cycles).

Figure 3 shows the evolution of shaft resistance during the cycles. Two different regimes can be identified. For the first 50 to 100 cycles, shaft resistance slightly decreases (of about 15 N), whereas it increases continuously and significantly for the subsequent load cycles. When the tip is at $\pm$0.5 mm the curves show a peak, which becomes increasingly marked with increasing number of cycles. As part of the national project SOLlicitations CYcliques sur Pieux de fondation (SOLCYP), Tali (2011) and Silva (2014) also reported an initial phase of 'cyclic softening' followed by a phase of 'cyclic hardening' for displacement-controlled cyclic loading tests carried out on a pile-probe jacked into large size samples of sand.

Table 1. Glageon sand properties

Grain shape	Volumetric weight kN/m^3	D_{50} mm	Coefficient of uniformity(C_u)	e_{max}	e_{min}
Angular	26.54	1.125	1.25	1.070	0.839

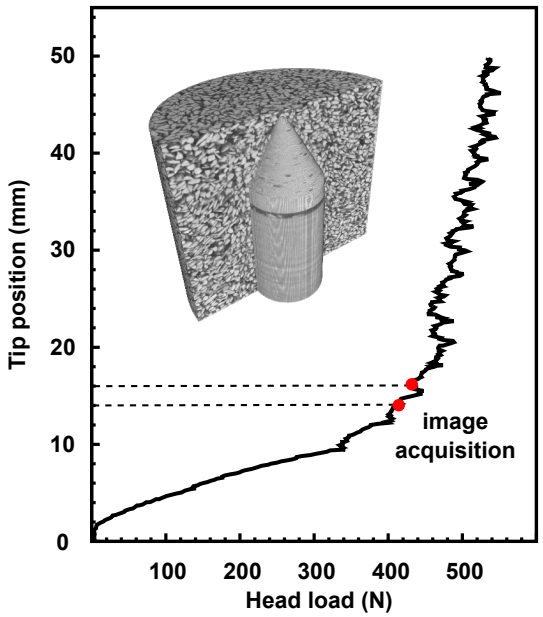

Figure 2. Sketch of a typical head load profile during pile installation inside the mini-calibration chamber. Points show an example of loading interruption for image acquisition, as illustrated by the 3D rendering recorded in 'local' tomography.

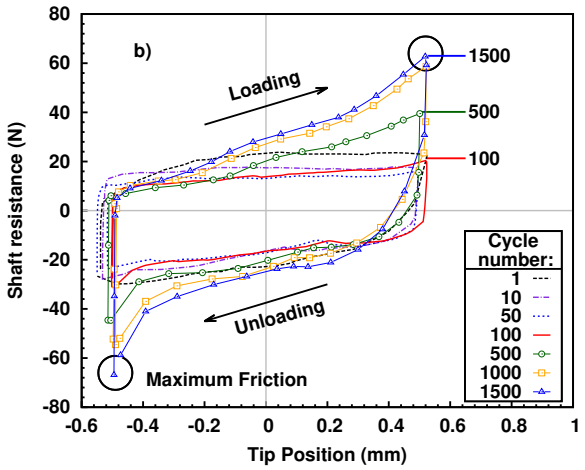

Figure 3. Evolution of shaft resistance during cycles with an amplitude of $\pm$0.5 mm (arrows show the loading path).

5 SELECTED RESULTS AT THE GRAIN-SCALE

5.1 *Volumetric behaviour*

Figure 4a shows the 3D porosity field at the initial state, *i.e.*, before pile embedment. Different layers of lower porosity, of about 40 %, are observed. These layers are attributed to the sand deposition process (layer by layer with slight tamping). Vertical slices taken through the volume at different stages of the test show lower porosity values on the boundaries of the specimen likely due to beam hardening effect, which leads to brighter voxels at the edges of a scanned object despite its homogeneity.

Figure 4b shows a relatively uniform porosity prior to testing, ranging from 44 to 49 %, which is consistent with the overall specimen porosity of about 45 % measured macroscopically during sample preparation. After pile installation, a zone ahead of the pile tip exhibits higher porosity values, of about 50 % (Fig. 4c), which indicates a loosening of the soil as reported by Chong (1988) and Silva & Combe (2014). A thin layer of low porosity (inferior to 33 %) is formed around the pile tip. This layer is likely due to the presence of fines produced by grain crushing during the installation and associated with a local densification. After 500 cycles, this layer becomes wider and extends along the shaft. A more detailed quantitative study of local density changes during cyclic loading can be found in Doreau-Malioche et al. (2018).

5.2 *Individual grain kinematics*

Figures 5a, b show individual grain displacements from discrete Digital Image Correlation (DIC), plotted in a vertical plane passing through the pile axis, between two loading increments during pile installation. Different regions where displacements concentrate can be identified (regions I, II and III). In region I, which goes until two pile radius ahead of the pile tip, vertical displacements dominate. In region II, beneath the pile tip, grains move away from the pile as the pile advances, with a high radial component. In region III, grains move in the opposite direction, towards the shaft. This distinct behavior, highlighted by the individual displacement vectors in Figure 5c, indicates a sand flow in the vicinity of the pile. The locations where the pile tip is not in contact with any grain are believed to be related to grain crushing. Grains that could not be tracked with DIC are not displayed and may be the grains crushed during the studied loading step. These results are in good agreement with the one obtained thanks to continuum DIC by Arshad et al. (2014) and Silva & Combe (2014).

For the study of the loading cycles, two pairs of 3D images were analysed, one from 10 to 50 cycles

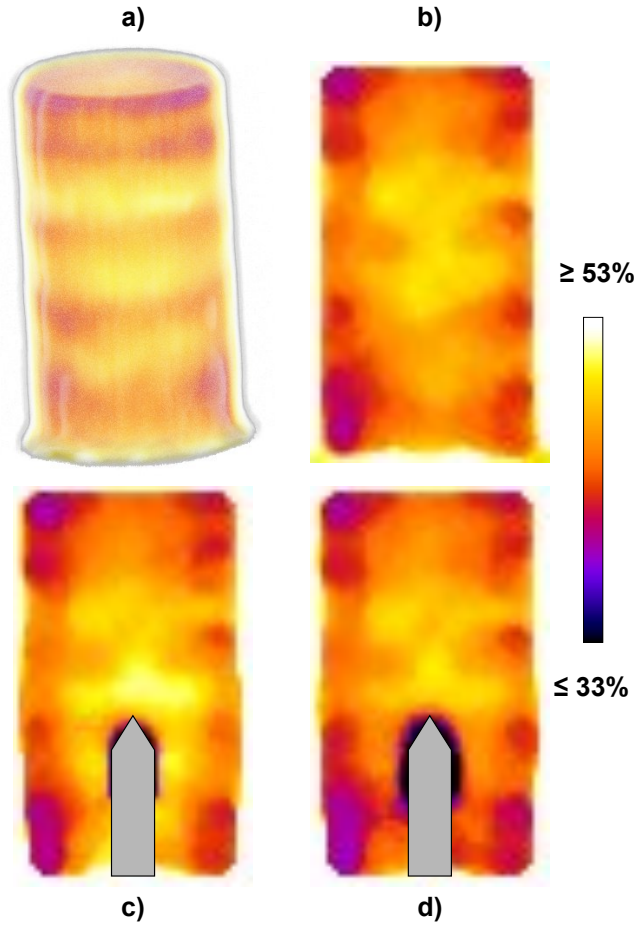

Figure 4. a) 3D field of porosity prior to testing (sample prepared with an initial density of 110%). Vertical slices taken through the 3D field of porosity b) prior to testing, c) after pile installation and d) after 500 cycles.

and one from 500 to 1000 cycles. It should be noted that these two increments respectively fall in the first and second regime of behaviour defined in Subsection 'Cyclic loading'. Individual displacement vectors for both loading increments are shown in Figures 6a, b. Ahead of the pile tip, the displacement vectors are nearly vertical and relatively minute, while around the shaft the displacement vectors have a much larger radial component. Grains move globally towards the shaft for both loading steps associated with a significant radial contraction as illustrated in Figure 4d. By comparing vertical and horizontal displacement fields after 50 and 1000 cycles, two different behaviours can be observed. The first 50 cycles cause high grain movements within a larger area around the shaft whereas, in the second regime, grains hardly move. In the first increment (Fig. 6a), grains are moving downwards. This is likely due to a reduction of the hoop stresses created during pile installation. This effect is erased in the later increment.

5.3 *Grains orientations*

The binarized images were also used to determine the center of mass and the inertia tensor of each individual grain following the method described by . The minor eigenvector of the inertia tensor, associated with the smallest eigenvalue, points in the longest direction of the grain, from the center of mass (it represents the axis around which the rotation of the grain is the less 'energy-demanding'). Given the elongated shape of Glageon grains, the minor eigenvector ($\mathbf{v_{min}}$) was selected as a meaningful measure to characterize grains orientations prior to and after pile installation. Thus, the orientation of a single grain θ was defined as the angle between $\mathbf{v_{min}}$ and the vertical axis, which also represents the pile axis denoted **z**.
As a result of the axisymmetry around **z**, the distribution of the orientations can be expressed by the probability density function of cosθ = x, denoted p(x), with $0 \leq \theta \leq \pi$. By construction, p is an even function, constant for an isotropic system. Such a function can be expanded in the series of Legendre polynomials, with only terms of even order, truncated after the 4^{th} order

$$p(x) = 1 + A(3x^2 - 1) + B(35x^4 - 30x^2 + 3) \quad (1)$$

in which the coefficients A and B are related to the moments of the distribution

$$A = \frac{15}{4}(\langle x^2 \rangle - \frac{1}{3})$$
$$B = \frac{9}{64}(35\langle x^4 \rangle - 30\langle x^2 \rangle + 3) \quad (2)$$

Coefficient 'A' can be used to describe the anisotropy of the distribution as it is directly related to the difference between the second moment and its isotropic value. This method has been proposed in a number of numerical studies to analyze the interparticle contacts anisotropy in a granular assembly (*e.g.*, Emam et al. 2006, Khalili et al. 2017).
Figure 7 shows the normalized distribution of grains orientations within a subdomain obtained by revolution of the cross section shown in Figure 7a prior to (Fig. 7b) and after pile installation (Fig. 7c). The results show that expansion (Eq. 1) achieves a good fit of the distribution in both cases. There is also a clear evolution of the distribution before and after pile installation. The sample is initially rather anisotropic. Grains are preferably oriented in the horizontal direction (cosθ close to 1), likely due to the sand deposition procedure. After pile installation, grains are reoriented alongside the pile . The number of grains with cosθ closer to zero increases, which leads to a more isotropic state ($\langle x^2 \rangle - \frac{1}{3}$ tends to zero).

6 CONCLUSIONS

X-ray tomography and 3D image analysis were used to investigate the effects of pile installation and loading cycles on sand-pile interface at the grain scale,

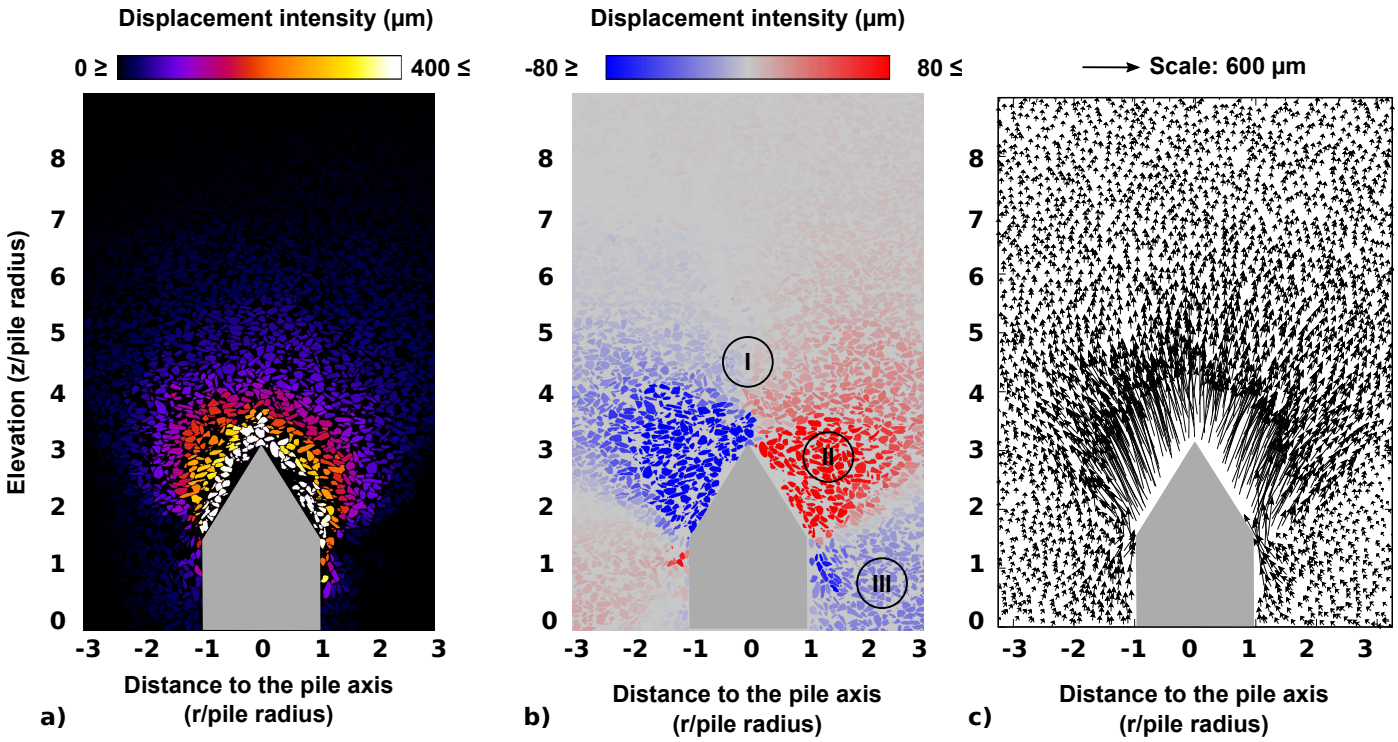

Figure 5. Typical individual grain displacements from discrete Digital Image Correlation (DIC), plotted in a vertical plane passing through the pile axis, for an incremental pile displacement of 1 mm: a) vertical displacements; b) horizontal displacements; c) individual displacement vectors for the same loading increment.

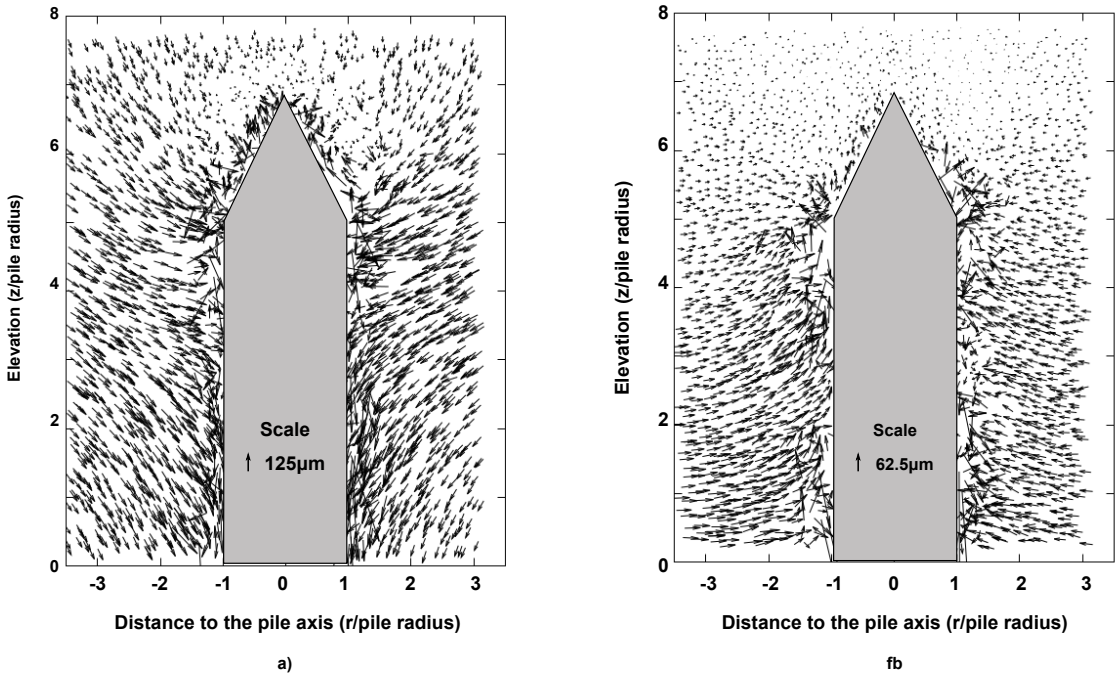

Figure 6. Individual displacement vectors obtained by discrete DIC a) between Cycle 10 and Cycle 50 and b) between Cycle 500 and Cycle 1000 (note that the scale is not the same for a and b).

within a mini-calibration chamber. Porosity measurements revealed a significant dilation around the pile during installation, followed by a local densification at the interface during subsequent cycles. 3D discrete DIC allowed the identification of different zones of displacement during pile installation. Two different kinematic responses of the sand mass, in the vivinity of the pile, were associated with the two regimes in shaft resistance evolution measured macroscopically during cyclic loading. Finally, preliminary results showed the ability to follow the evolution of anisotropy in terms of grains orientations during mechanical loading. Further analysis of grains orientations can provide valuable information to understand the interface response within a single cycle.

In this experimental study, the test conditions are admittedly not representative of true field conditions. However, the macroscopic response of the interface in the mini-calibration chamber is consistent with the one obtained in a previous study carried out at a larger

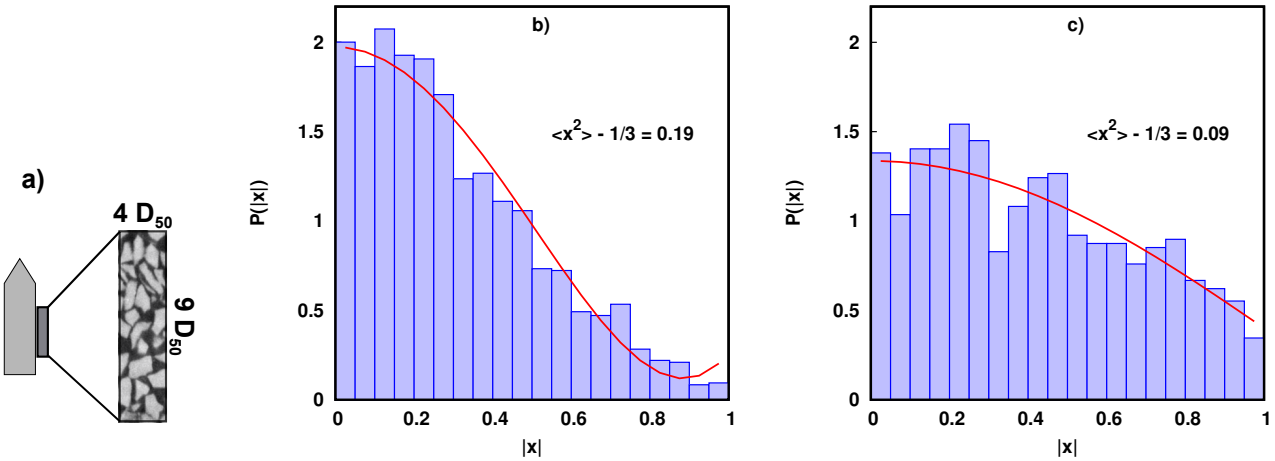

Figure 7. a) Schematic of the cross-section defining the subdomain over which the orientations are studied. Distributions of grains orientations with its representation truncated at the 4^{th} order b) pior to and c) after pile installation.

scale within the large calibration chamber of Laboratoire 3SR. These results indicate that the size effects do not affect the main grain-scale mechanisms driving the macroscopic behaviour of the sand-pile interface. The small scale study offers new possibilities in terms of quantitative analysis of the behaviour of the sand grains at the interface, which can be used to validate grain-scale numerical models.

7 ACKNOWLEDGEMENTS

The authors gratefully acknowledge Pascal Charrier, Christophe Dano, from Laboratoire 3SR, for their contributions. Laboratoire 3SR is part of the LabEx Tec 21 (Investissements dAvenir grant agreement number ANR-11-LABX-0030).

REFERENCES

Arshad, M. F., Tehrani, S. Prezzi, M. & Salgado, R. (2014). Experimental study of cone penetration in silica sand using digital image correlation. *Géotechnique 64 (7)*, 551–569.

Chong, M. (1988). Density changes of sand on cone penetration resistance. *First international symposium on penetration testing ISOPT-1*, Rotterdam/Balkema, vol. 2, pp. 707714.

Doreau-Malioche, J., Combe, G., Viggiani, G. & Toni, J. B. (2018). Shaft friction changes for cyclically loaded displacement piles: an x-ray investigation. *Géotechnique Letters*, DOI: 10.1680/jgele.17.00141.

Emam, S., Canou, J., Corfdir, A., Dupla, J. C. & Roux, J. N. (2018). Elaboration et comportement mécanique de matériaux granulaires solides modèles: expériences et simulations numériques. In B. Cazacliu and J.N. Roux (ed.) *Rhéologie des pâtes et des matériaux granulaires, Paris, France*, volume SI12 of Etudes et Recherches des Laboratoires des Ponts et Chaussées, Presses du Laboratoire Central des Ponts et Chaussées, pp. 105-145.

Fioravante, V. (2002). On the shaft friction modelling of non-displacement piles in sand. *Soils Found. 42 (2)*, 23–33.

Hebeler, G. L., Martinez, A. & Frost, J. D. (2015). Shear zone evolution of granular soils in contact with conventional and textured CPT friction sleeves. *KSCE J. Civil Engng. 20 (4)*, 1267–1282.

Khalili, M. H., Roux, J. N., Pereira, J. M., Brisard, S. & Bornert, M. (2017). Numerical study of one-dimensional compression of granular materials. I.Stress-strain behavior, microstructure, and irreversibility. *Phys. Rev 95*, DOI: 10.1103/PhysRevE.95.032907.

Schindelin, J., Arganda-Carreras, I. & Frise, E. (2012). Fiji: an open-source platform for biological-image analysis. *Nature methods 9 (7)*, 676–682, PMID 22743772, doi:10.1038/nmeth.2019.

Silva, M. (2014). Experimental study of ageing and axial cyclic loading effect on shaft friction along driven piles in sand. *PhD Thesis*, Université de Grenoble, France.

Silva, M. & Combe, G. (2014). Sand displacement field analysis during pile installation using x-ray tomography and digital image correlation. *International Symposium on Geomechanics from Micro to Macro, Cambridge, UK*, CRC Press/Balkema, vol. 1, pp. 15991603.

Silva, M., Combe, G., Foray, P., Flin, F. & Lesaffre, B. (2013). Postmortem Analysis of Sand Grain Crushing From Pile Interface Using X-ray Tomography. In *AIP Conf. Proc. Powders and Grains, Sydney, Australia*. UNSW, vol. 1542, pp. 297-300.

Tali, B. (2011). Comportement de l'interface sols-structure sous sollicitations cycliques : application au calcul des fondations profondes. *PhD Thesis*, Université de Paris Est, France.

Tehrani, F. S., Han, F., Salgado, R., Prezzi, M., Tovar, R. D. & Castro, A. G. (2016). Effect of surface roughness on the shaft resistance of non-displacement piles embedded in sand. *Géotechnique 66 (5)*, 386–400.

Tsuha, C. H. C., Foray, P. Y., Jardine, R. J., Yang, Z. X., Silva, M. & Rimoy, S. (2012). Behaviour of displacement piles in sand under cyclic axial loading. *Soils Found. 52 (3)*, 393–410.

Tudisco, E., Andò, E., Cailletaud, R. & Hall, S. A. A local Digital Volume Correlation code. *SoftwareXC 6*, 267–270.

White, D., & Bolton, M. (2002). Observing friction fatigue on a jacked pile. In Springman S. M. (ed.) *Constitutive and Centrifuge Modeling: Two Extremes*, Rotterdam/Balkema, pp. 347354.

Yang, L., Jardine, R., Zhu, B., Foray, P. & Tsuha, C. (2010). Sand grain crushing and interface shearing during displacement pile installation in sand. *Géotechnique 60 (6)*, 469–482.